



# Dynamic Optimization of a Steerable Screw In-pipe Inspection Robot Using HJB and Turbine Installation

H. Tourajizadeh\*, V. Boomeri, M. Rezaei and A. Sedigh

*Mechanical Engineering Department, Faculty of Engineering, Kharazmi University, Tehran, Iran*

(Accepted December 10, 2019. First published online: January 16, 2020)

## SUMMARY

In this paper, two strategies are proposed to optimize the energy consumption of a new screw in-pipe inspection robot which is steerable. In the first method, optimization is performed using the optimal path planning and implementing the Hamilton–Jacobi–Bellman (HJB) method. Since the number of actuators is more than the number of degrees of freedom of the system for the proposed steerable case, it is possible to minimize the energy consumption by the aid of the dynamics of the system. In the second method, the mechanics of the robot is modified by installing some turbine blades through which the drag force of the pipeline fluid can be employed to decrease the required propulsion force of the robot. It is shown that using both of the mentioned improvements, that is, using HJB formulation for the steerable robot and installing the turbine blades can significantly save power and energy. However, it will be shown that for the latter case this improvement is extremely dependent on the alignment of the fluid stream direction with respect to the direction of the robot velocity, while this optimization is independent of this case for the former strategy. On the other hand, the path planning dictates a special pattern of speed functionality while for the robot equipped by blades, saving the energy is possible for any desired input path. The correctness of the modeling is verified by comparing the results of MATLAB and ADAMS, while the efficiency of the proposed optimization algorithms is checked by the aid of some analytic and comparative simulations.

**KEYWORDS:** In-pipe inspection robot; Optimal control; Energy harvesting; Optimal modeling.

## 1. Introduction

In-pipe inspection robots (IPIRs) are among the new generation mobile robots that are designed to move through the pipeline installations in order to detect and inspect any pipeline bugs. Modeling and control of such robots are the focus of new researchers since they are extremely important toward handling the inspection and even manipulation within the pipeline in which a human being is not able to enter or perform any operational task. This limitation is the result of the size of the pipes, their probable dangerous contents, flowing fluid stream, etc. Varieties of in-pipe model inspection robot with different locomotion mechanism and different degrees of freedom (DOF) are proposed, which is suitable for specific tasks. The origin of these kind of robots can be referred to mobile robots as the first generation of these type of robots from which their primary formulations are derived. In recent years, a significant volume of research has been focused on the improvement of mobile robots and lots of approaches are proposed for tracking, controlling, and optimization of these kinds of robots. Peng et al.<sup>1</sup> investigated the adaptive distributed formation control problem for multiple nonholonomic wheeled mobile robots. Scaglia et al.<sup>2</sup> studied the problem of mobile robots under uncertainties. Simba et al.<sup>3</sup> focused on generating smooth trajectories using piecewise Bezier curves

\* Corresponding author. E-mail: [Tourajizadeh@khu.ac.ir](mailto:Tourajizadeh@khu.ac.ir)

for a wheeled nonholonomic mobile robot. Filaretov and Pryanichnikov<sup>4</sup> addressed an innovative technology used for mobile robots. Liu and Jiang<sup>5</sup> proposed a new class of distributed nonlinear controllers for leader-following formation control of unicycle nonholonomic robots without global position measurements.

Although the mobility of these kinds of robots is high and their ability to do a variety of tasks is increased, however, these kinds of robots are not appropriate for moving through the pipelines since they cannot remain stable in the pipes especially during steering periods. So researchers have promoted the design of mobile robots in order to increase their ability to move through the pipes and investigate the lines. The new generation robots is more suitable in order to investigate the internal space of the pipes and detect the cracks, leaks, and implement of non-destructive tests on them. These kinds of robots are called IPIRs and they are divided into three main categories: (1) without wheel robots, (2) caterpillar robots, and (3) wheel-based robots. All of these groups are also divided into some subgroups. Numerous types of in-pipe robots have been designed so far. Takahashi et al.<sup>6</sup> designed a robot based on earthworm motion that is composed of three locomotive units. Suzumori et al.<sup>7</sup> designed an in-pipe robot called "snaking drive" that can adapt itself with pipes' diameter. Zagler and Pfeiffer<sup>8</sup> designed a leg-based-type robot (MORITZ) which can climb through the pipes with different rates of inclinations. These kind of robots were too slow, so a new generation of these robots was developed with wheel and caterpillar. Caterpillar robots provide stronger propulsion friction compared to wheeled-based ones. Kim et al.<sup>9</sup> designed a caterpillar-based in-pipe robot (wall pressed type) to provide a good friction force between the robot and pipes. This robot is able to climb through vertical pipes as a result of its wall-pressed mechanism. Harish and Venkateswarlu<sup>10</sup> designed a robot with caterpillar wheels which consists of a complementary metal oxide semiconductor camera, an accelerometer, a temperature sensor, and a ZigBee module. Also, the kinematics of the robot is considered in this paper. Suzumori et al.<sup>11</sup> developed a micro inspection robot for an in-pipe robot equipped by a high-quality micro charge-coupled device camera and a dual hand for manipulating small objects in the pipes. Nagaya et al.<sup>12</sup> proposed a simple caterpillar robot with a new feature, that is, magnetic caterpillar that provides the ability to move through the vertical pipes and also increased the robot's stability. To design a flexible robot, Ciszewski et al.<sup>13</sup> presented a robot with a new mechanism to operate in circular and rectangular pipes and ducts oriented horizontally and vertically. Kwon and Yi<sup>14</sup> designed a new caterpillar robot in order to provide a good frictional condition between the pipe's wall and the robot system. It also uses a differential drive to steer the robot and spring-loaded four-bar mechanisms to assure the leg's suspension with respect to the pipes' wall. In order to increase the adaptability of the robot with the geometrical condition of the pipes, Park et al.<sup>15</sup> proposed a caterpillar robot that can adapt itself with pipe diameter. It also has an angular sensor to sense the curvature of the pipes during turning of the robot. Despite good maneuverability of caterpillar robots as a result of their acceptable rate of friction, their stability and adaptability with respect to different pipeline geometrical shapes are not good. Wheeled based in-pipe robots seem to be a better solution to deal with the mentioned challenges. Zhang and Yan<sup>16</sup> designed a wheeled robot with active pipe-diameter adaptability. They modeled the system and extracted the related differential equations. Afterward, the robot is controlled using Proportional & Derivative and Proportional & Integrator & Derivative controllers. Roh and Choi<sup>17</sup> proposed a wheeled wall press in-pipe robot with a miniature differential drive. The mechanism of differential drive is designed considering steerability to increase the adaptability of the robot with any pipeline configurations. Dertien et al.<sup>18</sup> discuss about the design of the wheeled robots that is omnidirectional and has active stabilizing control.

Wheeled robots with wall-press mechanism are so useful to increase the adaptability of the robot with respect to the pipe shape, but screwdrive mechanism of locomotion provides a more optimal mechanism with lower cost and equipment for practical applications. Screw-based locomotion in-pipe robots are considered the most effective and optimal mechanism of these kinds of robots since they can provide strong stability with good maneuverability using the least number of DOF. Peng Li et al.<sup>19</sup> designed an in-pipe inspection robot equipped with one driving motor that is the main body of the Multifunctional Mobile Unit (MMU<sup>1</sup>). They developed three kinds of MMU by installing different assemblies on the proposed versatile platform. Kakogawa and Ma<sup>20</sup> presented a motion analysis of an in-pipe robot with a screwdrive mechanism. Zhang et al.<sup>21</sup> proposed a flexible

<sup>1</sup> *Multifunctional Mobile Units.*

steering mechanism in order to move through the branches of the pipes. Although they investigated the curved-shaped pipes in this paper, the dynamics of the system is not extracted.

However, the ordinary screw-based in-pipe robots are not able to change their pitch rate, and this limitation avoids them from the possibility of obstacle avoidance. The proposed screw in-pipe robot in this paper has a steerable wheel by which the pitch rate of the robot locomotion is adjustable and as a result, the obstacles can be bypassed. Increasing the number of actuators of the robot while the DOF is fixed provides the possibility of optimal control of the robot. Some optimal control strategies are proposed in<sup>22</sup> for an in-pipe robot. This kind of in-pipe robot is able to move through any inclined angle pipe using adjustable screw rollers. However, in this robot, the angle of the rollers are passive and it is not possible to control them in an active way or employ it toward optimal path planning of the robot. Different kinds of optimal controls are studied in the literatures for robots with different structures. Two general approaches toward the optimization of the robot performance are optimal path planning and energy harvesting. In the first approach, the optimal path of the robot is extracted using variation methods and considering a predefined cost function. However, in the latter case, a portion of dissipated energy is regenerated by the aid of some assistive mechanism installed on the system. One of the most powerful optimization tools for optimal control of the robots is Hamilton–Jacobi–Bellman (HJB). This method is just implemented for mobile robots by Korayem et al.,<sup>23</sup> through which the optimal path is extracted in order to minimize the consumed energy. Adel Abbaspour et al.<sup>24</sup> presented the optimal formation of a group of the wheel-based robot that is dealt with for manipulating a common object. Mohamed Boukens et al.<sup>25</sup> performed the trajectory tracking and solved optimal control problem of mobile robot systems with nonholonomic constraints, in the presence of time-varying parametric uncertainties and external disturbances. Jinu Krishnan et al.<sup>26</sup> worked on the path planning problem for a single autonomous robot treading on a static terrain by using optimal control theory. Jihee Han<sup>27</sup> proposed a new method to solve the path planning problem in two steps. First, the surrounding point set (SPS) is determined where the obstacles are circumscribed by these points. Afterward the initial feasible path is generated based on the SPS. Rui-Zhuo Song et al.<sup>28</sup> proposed a new method to solve the optimal tracking control of continuous-time systems based on the HJB equation. The performance index function is a compromise of the state error and the controlling effort. Dipak M. Adhyaru et al.<sup>29</sup> proposed the HJB optimal control algorithm for improving the performance of a robust controller of a nonlinear system. Utilizing the Lyapunov direct method, the controller is shown to be optimal with respect to a cost function that includes a maximum bound for the system uncertainty.

On the other hand, energy harvesting is not yet considered for this kind of robots. The best solution to save the energy of such a system is employing turbine blades on the system. Implementation of these blades in order to increase the propulsion power of the system is just studied for underwater vehicles and is not employed for robots so far. Andrzej Sioma<sup>30</sup> presented the design of the water propulsion system. Particular attention was paid to the use of paddling techniques and water jet power. Benedetto Allotta et al.<sup>31</sup> worked on autonomy, performances, and maneuverability of underwater vehicles by the features of their propulsion layouts. Ehsan Zakeri et al.<sup>32</sup> presented a dynamic modeling and robust control of a mini unmanned underwater vehicle equipped with a new arrangement of water jet propulsion.

So it can be seen that energy harvesting using turbine blades and also optimization of screw in-pipe robots using optimal control strategies have been ignored so far. In this paper, optimal control of the mentioned steerable screw in-pipe inspection robot is performed and its performance is compared with the robot in which the energy harvesting method is employed to optimize the response of the system. First of all, in the next section, kinematic and kinetic modeling of the new proposed steerable in-pipe inspection robot is represented. Afterward, in section three, the robot is controlled using a robust sliding mode controller (SMC) to neutralize the destructive effects of disturbances and uncertainties. In section four, two strategies of energy optimization are introduced including installing turbine blades on the robot and planning the optimal path. Some turbine-shaped blades are installed on the rotor part of the robot and the formulation of the robot model is improved accordingly. Drag force of the fluid flow of the pipeline stream is added to the formulation as the external input, and it is shown that according to the specific proposed installation of the turbine blades on the rotor of the robot, the exerted drag force can be converted to propulsion torque for the in-pipe robot and the rate of energy harvested is evaluated. At the second strategy, the dynamic formulation of the ordinary in-pipe robot without the mentioned blades are employed for HJB optimization method and the optimal

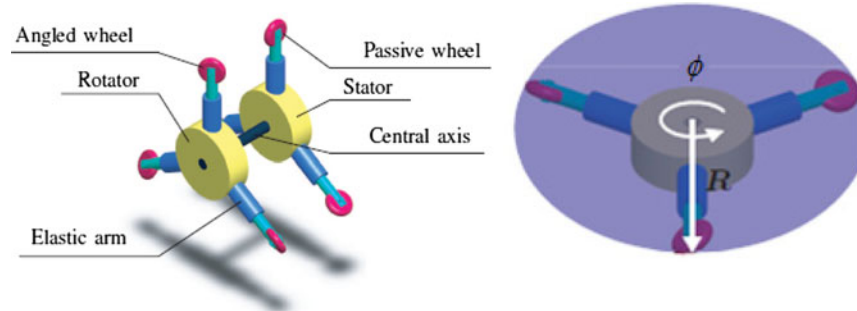


Fig. 1. An in-pipe screw robot.<sup>20</sup>

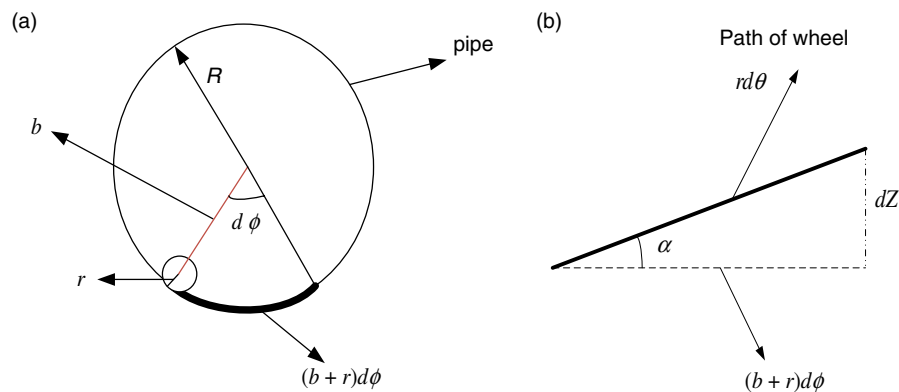


Fig. 2. (a) Frontal view of the robot the pipe. (b) The differential element of the motion of the wheel.

input of the system is calculated according to variation in the system dynamics. It is shown again that this input is optimum compared to ordinary computed torque method. At the last section, the correctness of the modeling and controller are verified by the aid of some simulation in MATLAB and the results are compared with previous studies. Finally, the efficiency of the proposed optimization strategies are investigated and some comparison studies are performed between the proposed approaches with respect to previous researches.

## 2. Methodology

In this section, the proposed in-pipe robot with two controlling inputs is introduced and its related modeling is represented. Then a robust controller based on sliding mode is employed to control the robot in the presence of external disturbances of fluid drag. Afterward, two optimization approaches based on energy harvesting and variation method will be implemented on the proposed multi-input in-pipe robot.

### 2.1. Modeling of the proposed robot

Scheme of an ordinary screw in-pipe inspection robot is depicted in Fig. 1. The angled wheel in this paper is promoted to an active actuator. In this section, the kinematic and kinetic models of this robot are represented.

This modeling is valid for both of the simple robots and of the one which is equipped by turbine blades since the active joint space parameters and the DOF are the same for both cases. Here by rotating the rotor section, the stator has a translational movement through the pipe.  $b$  is the length between the center of the robot and the center of the wheel,  $r$  is the radius of the wheels; and thus according to Fig. 2, we have  $R = (r + b)$  which is the radius of the pipe.  $\phi$  is the angle of the hull,  $\theta$  is the angle of the rotation of the wheels, and  $\alpha$  is the inclined angle of the wheels. The front wheel of the proposed system is steerable using an active actuator in contrast with the one which is introduced in.<sup>20</sup> Thus, the corresponding pitch rate can be changed through which the ordinary obstacles could be avoided.

It can be shown that the relation between the joint space velocity and workspace ones can be presented as Eq. (1). Here  $\dot{x}$ ,  $\dot{y}$ ,  $\dot{z}$  and  $\dot{\phi}$  are the work space parameters and  $\dot{\alpha}$  and  $\dot{\phi}$  are the joint space parameters. The Jacobian matrix ( $J$ ) in straight pipes can be extracted as Eq. (1):

$$\begin{pmatrix} \dot{x} \\ \dot{y} \\ \dot{z} \\ \dot{\phi} \end{pmatrix} = \begin{bmatrix} 0 & 0 \\ 0 & 0 \\ 0 & R \tan(\alpha) \\ 0 & 1 \end{bmatrix} \begin{pmatrix} \dot{\alpha} \\ \dot{\phi} \end{pmatrix} \tag{1}$$

In order to extract the dynamics of the robot, first the dynamics of the simple model is represented here and its generalized force is then improved to modify the formulation for the system equipped by the blades. The main generalized coordinates are considered as ( $\alpha$  and  $\phi$ ) and the related dynamic equation of the steerable screw in-pipe inspection robot without blades can be extracted as below using Lagrangian approach for the robot in the presence of fluid stream:<sup>33</sup>

$$\ddot{\phi} = \frac{\delta Rg(1 + \tan^2(\alpha))\dot{\alpha} - 2R^2\alpha_M \frac{S_\alpha}{C_\alpha^3} \dot{\alpha}\dot{\phi} - \Gamma\mu bF_N S_\alpha}{\Gamma\alpha_m b^2 + I_B + R^2\alpha_M \tan^2(\alpha)} + \frac{T_m}{\Gamma\alpha_m b^2 + I_B + R^2\alpha_M \tan^2(\alpha)} \tag{2}$$

$$\ddot{\alpha} = \left( \frac{R^2\alpha_M (\tan(\alpha) + \tan^3(\alpha))}{\Gamma I_{wheel}} \right) \dot{\phi}^2 - \left( \frac{\delta Rg (1 + \tan^2(\alpha))}{\Gamma I_{wheel}} \right) \dot{\phi} + \frac{T_s}{\Gamma I_{wheel}} \tag{3}$$

where

$$\alpha_M = \left( M_m + M_h + \Gamma m + \Gamma \frac{I_{WX}}{r^2} \right)$$

$$\alpha_m = \left( m + \frac{I_{WZ}}{r^2} \right)$$

Also,  $M_m$  and  $M_h$  are the mass of the motor and hull, respectively, and  $I_{WX}$  and  $I_{WZ}$  are the wheel moment of inertia about the  $X$  and  $Z$  axis.  $\delta$  is the summation of all masses and  $g$  is the gravity force.  $\Gamma$  denotes the number of steering wheels. Also  $C_\alpha$  and  $S_\alpha$  denote  $\cos(\alpha)$  and  $\sin(\alpha)$ ,  $I_{WZ}$ ,  $I_{WX}$ ,  $I_{wheel}$ , and  $I_B$  are the wheel moment of inertia around the pipe axis, wheel moment of inertia around the leg, and polar moment of inertia of the hull, respectively.  $T_s$  is the torque generated by the motor relevant to the steering wheels and  $T_m$  is the torque generated by the motor relevant to the hull.  $T_f = \Gamma b \mu F_N \sin(\alpha)$  is the resisting torque due to the friction between the wheels and their axles,  $r$  is the wheel radius,  $b$  is the length of wheel axis,  $\mu$  is the friction coefficient,  $F_N$  denotes the normal force exerted by the axles, and  $\Gamma$  is the number of active wheels. Also both of the joint spaces of the robot including the main propulsion and steering systems are fully actuated.

In order to solve the mentioned coupled equations, extracting the time responses of the DOF and finally controlling the system, it is required to rewrite the equations in the form of state space. Considering  $X = \{x_1; x_2; x_3; x_4\} = (\phi; \dot{\phi}; \alpha; \dot{\alpha})$  as the states of the proposed in-pipe robot, corresponding state space can be presented as:

$$\dot{x}_1 = x_2$$

$$\dot{x}_2 = \frac{\delta Rg(1 + \tan^2(x_3))x_4 - 2R^2\alpha_M \frac{S_{x_3}}{C_{x_3}^3} x_4 x_2 - \Gamma\mu bF_N S_{x_3}}{\Gamma\alpha_m b^2 + I_B + R^2\alpha_M \tan^2(x_3)} + \frac{T_m}{\Gamma\alpha_m b^2 + I_B + R^2\alpha_M \tan^2(x_3)} \tag{4}$$

$$\dot{x}_3 = x_4$$

$$\dot{x}_4 = \left( \frac{R^2\alpha_M (\tan(x_3) + \tan^3(x_3))}{\Gamma I_{wheel}} \right) x_2^2 - \left( \frac{\delta Rg (1 + \tan^2(x_3))}{\Gamma I_{wheel}} \right) x_2 + \frac{T_s}{\Gamma I_{wheel}}$$

### 2.2. Control scheme

Considering the fact that the drag force of the flowing fluid is an external disturbance for the robot, the sliding mode control approach is employed here in order to control and stabilize the system. The exact



nonlinear presentation of the state space of the proposed robot is shown in Eqs. (5) and (6). Also  $K_{f_1}\dot{\phi}$  and  $K_{f_2}\dot{\phi}$  describe the viscous friction implemented on the robot's hub and the wheels, respectively.  $x \in \mathbb{R}^n$  is the state vector,  $u \in \mathbb{R}^m$  represents controlling inputs of the system,  $y \in \mathbb{R}^m$  stands for outputs,  $f$  and  $g$  are nonlinear smooth vector fields,  $h$  is a nonlinear smooth scalar function, and  $d(t)$  is a bounded external disturbance with a definite bound of  $D$ , that is  $|d(t)| \leq D < \infty$ .<sup>32</sup>

$$\dot{X} = f(x) + g(x)u + d(t) = \begin{Bmatrix} x_2 \\ \frac{\delta Rg(1 + \tan^2(x_3))x_4 - 2R^2\alpha_M S_{x_3}x_4x_2 - \Gamma\mu bF_N S_{x_3} - K_f x_2}{\Gamma\alpha_m b^2 + I_B + R^2\alpha_M \tan^2(x_3)} \\ x_4 \\ \left(\frac{R^2\alpha_M (\tan(x_3) + \tan^3(x_3))}{\Gamma I_{wheels}}\right) x_2^2 - \left(\frac{\delta Rg(1 + \tan^2(x_3))}{\Gamma I_{wheels}}\right) x_2 \end{Bmatrix} + \begin{bmatrix} 0 & 0 \\ 1 & 0 \\ \frac{\Gamma\alpha_m b^2 + I_B + R^2\alpha_M \tan^2(x_3)}{0} & 0 \\ 0 & 1 \\ 0 & \frac{1}{\Gamma I_{wheels}} \end{bmatrix} \begin{bmatrix} T_m \\ T_s \end{bmatrix} + \begin{bmatrix} d(t) \\ 0 \end{bmatrix} \tag{5}$$

$$y = h(x) = \begin{bmatrix} x_1 \\ x_3 \end{bmatrix} \tag{6}$$

where

$$K_f = K_{f_1} + \frac{b+r}{rC_\alpha} K_{f_2}$$

Substituting the parameter of the present system, the control law  $u$  can be calculated as Eq. (7) according to sliding mode control:

$$u = -j^{-1}(x) \left( - \begin{bmatrix} L_f^{r_1} h_1(x) \\ \vdots \\ L_f^{r_m} h_m(x) \end{bmatrix} + g^{-1}(x) \begin{bmatrix} v_1 \\ \vdots \\ v_m \end{bmatrix} \right) = \begin{bmatrix} \frac{1}{\Gamma\alpha_m b^2 + I_B + R^2\alpha_M \tan^2(x_3)} & 0 \\ 0 & \frac{1}{\Gamma I_{wheels}} \end{bmatrix}^{-1} \left( \begin{bmatrix} \frac{\delta Rg(1 + \tan^2(x_3))x_4 - 2R^2\alpha_M S_{x_3}x_4x_2 - \Gamma\mu bF_N S_{x_3} - K_f x_2}{\Gamma\alpha_m b^2 + I_B + R^2\alpha_M \tan^2(x_3)} \\ \left(\frac{R^2\alpha_M (\tan(x_3) + \tan^3(x_3))}{\Gamma I_{wheels}}\right) x_2^2 - \left(\frac{\delta Rg(1 + \tan^2(x_3))}{\Gamma I_{wheels}}\right) x_2 \end{bmatrix} + \begin{bmatrix} v_1 \\ \vdots \\ v_m \end{bmatrix} \right) \tag{7}$$

where  $\bar{v} = [v_1 \dots v_m]^T$  is the new set of inputs that should be defined by the designer. To compute the required  $v$ , the desired sliding surface should be defined. Here the following sliding surfaces are considered to construct the sliding mode controlling input:

$$\begin{aligned} s_1 &= c_1(x_1 - x_{1d}) + c_2(\dot{x}_1 - \dot{x}_{1d}) \\ s_2 &= c'_1(x_2 - x_{2d}) + c'_2(\dot{x}_2 - \dot{x}_{2d}) \end{aligned} \tag{8}$$

Here  $c$  and  $c'$  are the coefficient of the two sliding paths, their related index number 1 and 2 denotes the position and velocity error of the states, and index  $d$  shows the desired path of the related state.

Based on Eq. (7), control law for the new proposed system can be presented in the following matrix form:

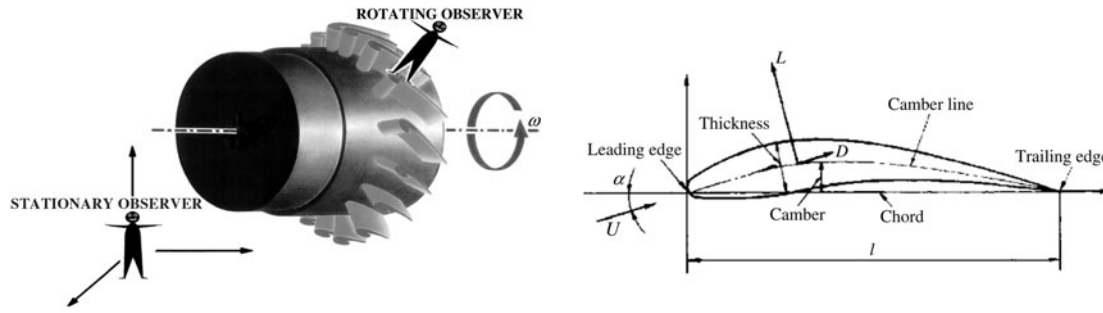


Fig. 3. Scheme of a turbine (left) and blade (right).<sup>33</sup>

$$\begin{bmatrix} u_1^* \\ u_2^* \end{bmatrix} = \begin{bmatrix} \frac{1}{\Gamma\alpha_m b^2 + I_B + R^2\alpha_M \tan^2(x_3)} & 0 \\ 0 & \frac{1}{\Gamma I_{wheels}} \end{bmatrix}^{-1} \left( \begin{array}{l} - \begin{bmatrix} c_1 \dot{e}_1 \\ c_1 \dot{e}_2 \end{bmatrix} - \begin{bmatrix} \frac{\delta R g (1 + \tan^2(x_3)) x_4 - \frac{2R^2\alpha_M S_{x_3} x_4 x_2}{\cos^3(x_3)} - \Gamma \mu b F_N S_{x_3} - K_f x_2}{\Gamma\alpha_m b^2 + I_B + R^2\alpha_M \tan^2(x_3)} \\ \left( \frac{R^2\alpha_M (\tan(x_3) + \tan^3(x_3))}{\Gamma I_{wheels}} \right) x_2^2 - \left( \frac{\delta R g (1 + \tan^2(x_3))}{\Gamma I_{wheels}} \right) x_2 \end{bmatrix} \\ d(t) + \begin{bmatrix} \ddot{x}_1 \\ \ddot{x}_3 \end{bmatrix} - \begin{bmatrix} \eta_{1\Delta} \operatorname{sgn}(s_1) \\ \eta_{2\Delta} \operatorname{sgn}(s_2) \end{bmatrix} \end{array} \right) \quad (9)$$

Here  $\bar{x}$  is the vector of the states and  $\eta_{\Delta} \geq \eta \geq 0$  should be defined by designer while the coefficient  $\eta$  is a positive constant satisfying the following equation  $\dot{s} \leq -\eta \operatorname{sgn}(s)$ .

### 2.3. Optimization of the designed robot

In order to optimize the energy consumption of the designed robot two procedures are employed in this paper. The former one is a kind of energy harvesting through installing turbine blades on the robot by which the drag force of the flowing fluid can be used as the propulsion force and so the required propulsion which should be provided by the aid of the motors can be reduced. The latter strategy is optimal path planning using variation method through which the optimal path of the robot can be planned in a way that results in a minimized value of objective function, considering the differential equations of the system.

**2.3.1. Modeling the robot with turbine blades.** In many applications, the robot needs to move within a full pipe through which the fluid is flowing. In this case, the drag force of the fluid should be considered as an external disturbance for the above-mentioned modeling and controlling procedure. In order to optimize the energy consumption of the robot through energy harvesting, it is proposed in this paper to employ fluid energy as the propulsion force of the robot. This importance can be easily realized by installing some turbine blades on the robot. For the case in which the direction of the robot movement is in the same direction of fluid flowing, it is obvious that the required external propulsion force of the robot is significantly reduced; however, it is proved in this paper that even for the case in in opposite direction, it is again possible to optimize the required controlling force if the turbine blades would be optimally designed and attached on the robot with an optimum angle. For both cases, the turbine converts the drag force of the fluid to a supporting torque by which, the required propulsion torque for the screw in-pipe robot can be strengthened. This concept is originally inspired by gas turbines. The following Fig. 3 shows a turbine blades together with its related blades.

In this case, the term  $n \frac{C_L R^2 l \rho v^2}{2}$  is the additive positive propulsion torque of the system. Here  $n$  is the number of blades,  $l$  is the blade length,  $\rho$  is the density of the fluid,  $v$  is the relative velocity of

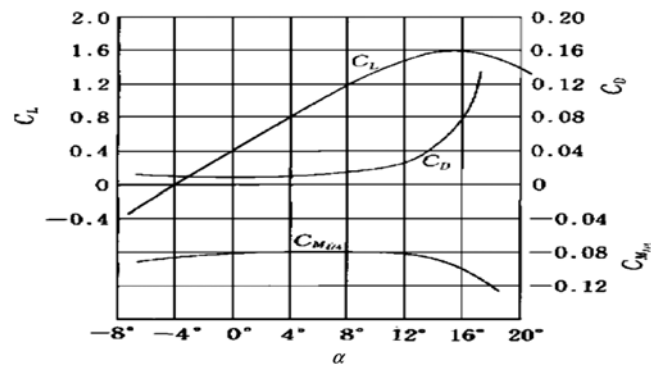


Fig. 4. Profile of the aerodynamic coefficients versus blade angles.<sup>33</sup>

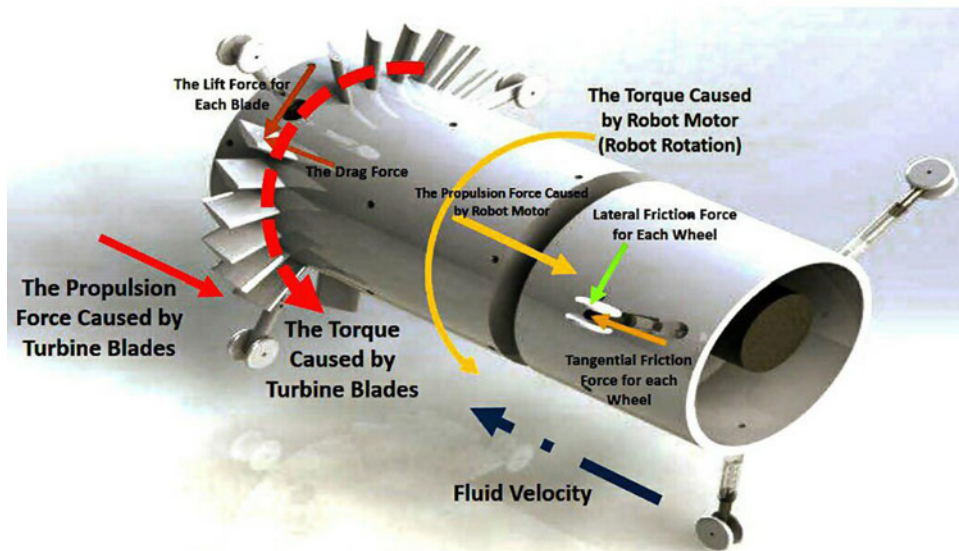


Fig. 5. Proposed in-pipe robot equipped by turbine blades.

the robot and fluid, and  $R'$  is the distance between the lift force and the center of the robot shaft. Generally, when a fluid flow impacts with a blade as shown in the above figure, a lifting force ( $L$ ) and a drag force ( $D$ ) will be produced. These two forces can be calculated as below:

$$L = \frac{C_L l \rho v^2}{2} \quad (10)$$

$$D = \frac{C_D l \rho v^2}{2} \quad (11)$$

Here it is desired to install the blades on the robot body in a way that results in the optimum positive propulsive torque even for the case that the fluid flow direction is opposite with respect to the robot movement direction. Figure 4 shows the relation between the lifting coefficient and drag coefficient versus different attachment angles of the blades.

It can be seen that for the optimum attachment angle which is between  $14^\circ$  and  $15^\circ$ , the lifting force which results in propulsive torque is about 40 times bigger than its related drag force which is resistive.

Thus, according to the above explanation, 18 blades with the mentioned optimum angle of  $15^\circ$  are installed on the front of the proposed in-pipe robot in a circular curve between the steerable wheels. The improved version of the proposed in-pipe robot with blades can be seen in Fig. 5.



As can be seen in the figure, the robot is moving against the fluid velocity. The rotational torque of the main motor related to the robot propulsion system provides a locomotion force against the fluid velocity as a result of frictional force of the robot wheels and its screw-shaped structure. It can be seen that in the improved version of this robot with the installed turbine blades again, the lift force of the flowing fluid on the blades results in a rotational torque on the robot in the same direction of the main propulsive motor of the robot. Thus, the resultant locomotion force related to this torque by the aid of the mentioned frictional force of the wheels and the screw shape structure of the robot will assist the main locomotion force of the robot in the same direction which finally decreases the required motor torque of the main motor. Thus, it can be concluded that the proposed improvement in the robot structure can significantly save the energy even for the case in which the robot is moving against the fluid velocity.

Considering the positive propulsive torque of the lifting force, the improved dynamics of the robot together with its attached blades can be rewritten as below:

$$\ddot{\phi} = \frac{\delta Rg(1 + \tan^2(\alpha))\dot{\alpha} - 2R^2\alpha_M \frac{S_\alpha}{C_\alpha^3} \dot{\alpha}\dot{\phi} - \Gamma\mu bF_N S_\alpha - K_f\dot{\phi} - \frac{AC_D b\rho \sin(\alpha) (R\dot{\phi} \sin(\alpha) + v)^2}{2}}{\Gamma\alpha_m b^2 + I_B + R^2\alpha_M \tan^2(\alpha)} + \frac{T_m + n \frac{C_L R' l \rho v^2}{2}}{\Gamma\alpha_m b^2 + I_B + R^2\alpha_M \tan^2(\alpha)} \tag{12}$$

$$\ddot{\alpha} = \left( \frac{R^2\alpha_M (\tan(\alpha) + \tan^3(\alpha))}{\Gamma I_{wheels}} \right) \dot{\phi}^2 - \left( \frac{\delta Rg (1 + \tan^2(\alpha))}{\Gamma I_{wheels}} \right) \dot{\phi} + \frac{T_s}{\Gamma I_{wheels}} \tag{13}$$

And the related state space of the robot considering the installed turbine blades can be expressed as follow:

$$\begin{aligned} \dot{x}_1 &= x_2 \\ \dot{x}_2 &= \frac{\delta Rg(1 + \tan^2(x_3))x_4 - 2R^2\alpha_M S_{x_3} x_4 x_2 - \Gamma\mu bF_N S_{x_3} - K_f x_2 - \frac{AC_D b\rho \sin(x_3) (R x_2 \sin(x_3) + v)^2}{2}}{\Gamma\alpha_m b^2 + I_B + R^2\alpha_M \tan^2(x_3)} + \frac{T_m + n \frac{C_L R' l \rho v^2}{2}}{\Gamma\alpha_m b^2 + I_B + R^2\alpha_M \tan^2(x_3)} \\ \dot{x}_3 &= x_4 \\ \dot{x}_4 &= \left( \frac{R^2\alpha_M (\tan(x_3) + \tan^3(x_3))}{\Gamma I_{wheels}} \right) x_2^2 - \left( \frac{\delta Rg (1 + \tan^2(x_3))}{\Gamma I_{wheels}} \right) x_2 + \frac{T_s}{\Gamma I_{wheels}} \end{aligned} \tag{14}$$

Here it should be considered that the optimization process has occurred on the structure of the system and the differential equation is changed accordingly. As it will be seen in the simulation section, this optimization has a steady-state optimality effect on the results.

**2.3.2. Optimal path planning.** The alternative solution toward the optimization of energy consumption of the robots as it was mentioned is calculating the optimal controlling input based on variation optimization method. This method was first proposed by Pontryagin and Bellman and the final method named HJB. Here it is desired to extract the controlling input in a way that a specific cost function could be optimized accordingly. The cost function is a function of the states and their related inputs, and the problem results in a series of coupled differential equations and its related boundary conditions. This method is basically an open-loop optimal control strategy through which the optimal path and its related controlling command can be calculated as a function of time. Implementation of the calculated optimal control for the robot will result in an optimal path through which the robot

motion requires the minimum amount of the desired objective function. It is first required in this method to define a cost function  $J$  and a Hamilton function  $H$  like below:

$$\begin{aligned}
 J &= h(x(t_f), t_f) + \int_{t_0}^{t_f} L(x(t), u(t), t) dt = \int (X^T Q_o X + u^T R_o u) dt; \\
 H(x(t), u(t), \lambda(t), t) &= L(x(t), u(t), t) + \lambda^T(t) [a(x(t), u(t), t)]
 \end{aligned}
 \tag{15}$$

where index  $f$  denotes the final value of the related parameter,  $u$  is the controlling effort,  $Q_o, R_o$  are optimization gains of states and input,  $a$  is the state space condition of the system and  $\lambda$  are known as co-states of the system which has the same number of the system states. The first part of the mentioned function is contributed to the final condition of the cost function, while the second term considers the cost function during the motion interval. This Hamilton function should be defined as Eq. (16) for the studied robot of this paper in order to minimize the error and energy of the system simultaneously.

$$\begin{aligned}
 J &= h(x(t_f), t_f) + \int_{t_0}^{t_f} L(x(t), u(t), t) dt = \int (X^T Q_o X + u^T R_o u) dt \\
 J &= \int_{t_0}^{\infty} \left( X^T \begin{bmatrix} 1 & 0 & 0 & 0 \\ 0 & 0 & 0 & 0 \\ 0 & 0 & 1 & 0 \\ 0 & 0 & 0 & 0 \end{bmatrix} X + u^T \begin{bmatrix} 0.01 & 0 \\ 0 & 0.1 \end{bmatrix} u \right) dt = \\
 J &= \int_{t_0}^{\infty} \left( \begin{bmatrix} \phi & \dot{\phi} & \alpha & \dot{\alpha} \end{bmatrix} \begin{bmatrix} 1 & 0 & 0 & 0 \\ 0 & 0 & 0 & 0 \\ 0 & 0 & 1 & 0 \\ 0 & 0 & 0 & 0 \end{bmatrix} \begin{bmatrix} \phi \\ \dot{\phi} \\ \alpha \\ \dot{\alpha} \end{bmatrix} + \begin{bmatrix} T_m & T_s \end{bmatrix} \begin{bmatrix} 0.01 & 0 \\ 0 & 0.1 \end{bmatrix} \begin{bmatrix} T_m \\ T_s \end{bmatrix} \right) dt
 \end{aligned}
 \tag{16}$$

Since the final condition is not independently significant for our case of study,  $h$  can be eliminated in the function and hence the related Hamilton function can be defined as:

$$\begin{aligned}
 H(x(t), u(t), \lambda(t), t) &= L(x(t), u(t), t) + \lambda^T(t) [a(x(t), u(t), t)] = \\
 &\left( \begin{bmatrix} \phi & \dot{\phi} & \alpha & \dot{\alpha} \end{bmatrix} \begin{bmatrix} 1 & 0 & 0 & 0 \\ 0 & 0 & 0 & 0 \\ 0 & 0 & 1 & 0 \\ 0 & 0 & 0 & 0 \end{bmatrix} \begin{bmatrix} \phi \\ \dot{\phi} \\ \alpha \\ \dot{\alpha} \end{bmatrix} + \begin{bmatrix} T_m & T_s \end{bmatrix} \begin{bmatrix} 0.01 & 0 \\ 0 & 0.1 \end{bmatrix} \begin{bmatrix} T_m \\ T_s \end{bmatrix} \right) + \\
 &\begin{bmatrix} \lambda_1 \\ \lambda_2 \\ \lambda_3 \\ \lambda_4 \end{bmatrix} [\dot{x}_1 \quad \dot{x}_2 \quad \dot{x}_3 \quad \dot{x}_4]
 \end{aligned}
 \tag{17}$$

Substituting the dynamics of the robot in the above formulation results in the following Hamiltonian function:

$$\begin{aligned}
 H &= \frac{I_w + \lambda_4 (R^2 \alpha_M \tan(x_3) + R^2 \alpha_M \tan^3(x_3))}{\Gamma} x_2^2 + \\
 &\left[ \lambda_1 - \frac{\lambda_2 \left( k_f + \frac{2R^2 \alpha_M x_4 S_{x_3}}{C_{x_3}^3} + \frac{AC_D R b \rho S_{x_3}^2}{2} \right)}{\Gamma \alpha_M b^2 + I_B - R^2 \alpha_M \tan^2(x_3)} - \frac{\delta I_w \lambda_4 g (b+r) (1 + \tan^2(x_3))}{\Gamma} \right] x_2
 \end{aligned}
 \tag{18}$$

$$\begin{aligned}
 & + \left[ \lambda_3 + \frac{\delta g \lambda_2 (b+r) (1 + \tan^2(x_3))}{\Gamma \alpha_m b^2 + I_B + R^2 \alpha_M \tan^2(x_3)} \right] x_4 + \frac{\lambda_2^2}{2 (\Gamma \alpha_m b^2 + I_B + R^2 \alpha_M \tan^2(x_3))^2} \\
 & \lambda_2 \left( \frac{\Gamma F_N b u S_{x_3} + \frac{A C_D b \rho v S_{x_3}}{2}}{\Gamma \alpha_m b^2 + I_B + R^2 \alpha_M \tan^2(x_3)} - \frac{\lambda_2}{(\Gamma \alpha_m b^2 + I_B + R^2 \alpha_M \tan^2(x_3))^2} \right)
 \end{aligned}$$

In the Hamiltonian function, the term of states and co-states of the system can be extracted using the following derivations:

$$\begin{aligned}
 \dot{\lambda}(t) &= -\frac{\partial H}{\partial x}(x(t), u(t), \lambda(t), t) \\
 \dot{x}(t) &= \frac{\partial H}{\partial \lambda}(x(t), u(t), \lambda(t), t)
 \end{aligned} \tag{19}$$

Also in order to extract the optimal value of the controlling input through which the optimal path can be realized, derivation of this function with respect to input is required:

$$\frac{\partial H}{\partial u}(x(t), u(t), \lambda(t), t) = 0 \tag{20}$$

Considering the above three series of the mentioned coupled of equations in which two sets of coupled differential equations appear, three sets of unknown variables, that is, optimal states, optimal co-states, and optimal controlling inputs can be calculated by the aid of  $2n$  boundary conditions of initial and final conditions of the system For  $n$  states, the number of the above differential equations is  $2n$  and they should be calculated using the following  $2n$  boundary conditions:

$$\begin{aligned}
 x(t_0) &= x_0 \\
 \left[ \frac{\partial h}{\partial x}(x(t_f), t_f) - \lambda(t_f) \right]^T \delta x_f + \left[ H(x(t_f), u(t_f), \lambda(t_f), t_f) + \frac{\partial h}{\partial t}(x(t_f), t_f) \right] \delta t_f &= 0
 \end{aligned} \tag{21}$$

The mentioned differential equations and its related boundaries are implemented for the dynamic equation of the presented robot of Eq. (14). Here it should be considered that the optimization process occurred on solving the differential equation, while the dynamic system itself is the same, and this fact as we will see in the simulation section results in transient optimality effect opposite to the former optimization method.

The overall flowchart of the mentioned path generator together with the designed robust controller can be depicted as Fig. 6 for the designed steerable in-pipe inspection robot.

Here the optimal path is calculated using the HJB method and this path is fed to the SMC controller to be tracked as the desired path. The drag force of the turbine blades can also be added to the controlling signal for the energy harvesting case.

### 3. Simulation Results

The correctness of the dynamic modeling and efficiency of the controlling system is verified by the same author in<sup>34</sup> by comparing the simulation results of MATLAB with ADAMS. Two scenarios are studied in this section. In the first scenario, the robot which is equipped by turbine blades is studied and its optimality will be evaluated. In the second scenario, the performance of an ordinary in-pipe robot is checked, while it is controlled through the optimal path extracted using the mentioned HJB method. In the end, these two methods are compared.

#### 3.1. Robot equipped by turbine blades

Consider a screw in-pipe inspection robot with the parametric characteristics of Table I.

Here the desired path of the robot with variable angle is a cylindrical path with variable pitch rate which can be controlled according to Eq. (22):

$$Z = R \varnothing \tan(\alpha) \tag{22}$$

Table I. The value of the physical parameters of the system.

Physical properties of the system			
Symbol	Value	Definition	Unit
$M$	0.01	Wheel mass	Kg
$M_h$	1	Hull mass	Kg
$M_m$	1	Motor mass	Kg
$r$	0.02	Wheel radius	m
$b$	0.1	Leg length	m
$A$	0.01	Robot's effective cross-sectional area	m <sup>2</sup>
$F_N$	15	The normal force of passive spring	N
$\mu$	0.2	Friction coefficient	–
$I_B$	10 <sup>-4</sup>	Hull's polar moment of inertia	Kg.m <sup>2</sup>
$I_{WZ}, I_{WX}$	10 <sup>-8</sup>	Wheel moment of inertia around the pipe axis	Kg.m <sup>2</sup>
$G$	9.8	Gravity	$\frac{m}{s^2}$
$\Gamma$	3	Number of active wheels	–
$I_{wheel}$	2*10 <sup>-8</sup>	Wheel moment of inertia around the leg	Kg.m <sup>2</sup>

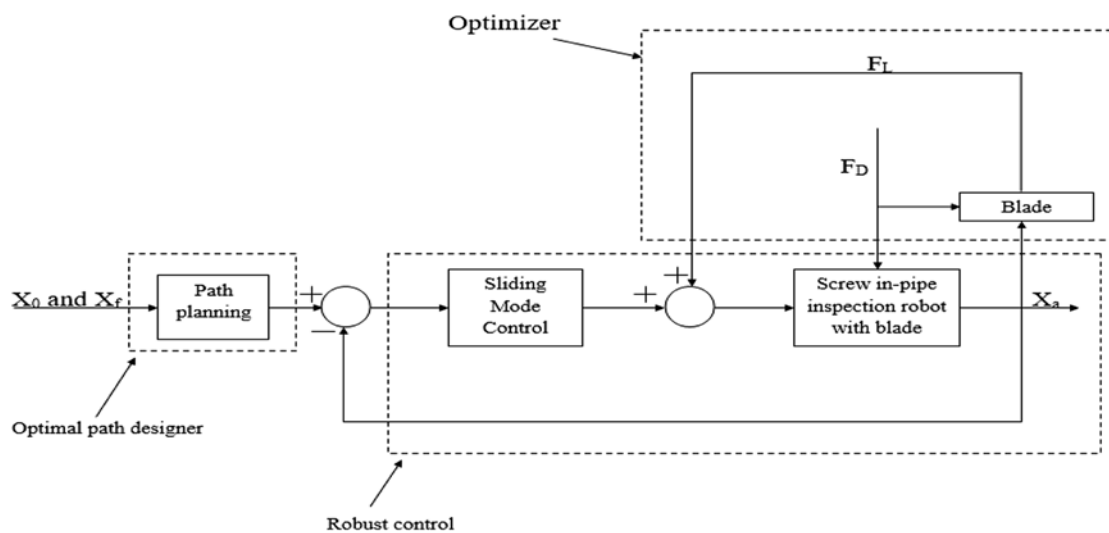


Fig. 6. Overall controlling scheme of the screw steerable in-pipe inspection robot equipped by sliding mode controller (SMC) controller which can be optimized using these two mentioned strategies.

Thus, the equations of the desired inputs of the states are:

$$x_1 = 0.5t \quad (23)$$

$$x_3 = 0.05t \quad (24)$$

The desired and actual trajectories of the robot joint space and its comparison for different velocities of the fluid and also its comparison with the response of the system without the mentioned turbine blades are shown in Fig. 6. As can be seen, the term  $3 \cdot 6v^2$ , which is related to the effect of the blade on the dynamics of the system, is a function of the fluid velocity. Figure 7 also shows the response of the system with and without the attached blades. In this scenario, the worst case is considered in which the direction of the fluid stream is in direction opposite to the robot movement.

The first figure demonstrates the effect of the blades on the position response of the first state. Since the velocity of the fluid affects directly on this state, we can conclude that the more the speed of the fluid is, the more the settling time of the state response increases with respect to its desired value which is related to the drag force of the stream. However, the difference is roughly ignorable. It can be seen that this effect cannot be observed for the third state since the effect of the fluid on this state is not highlighted here.

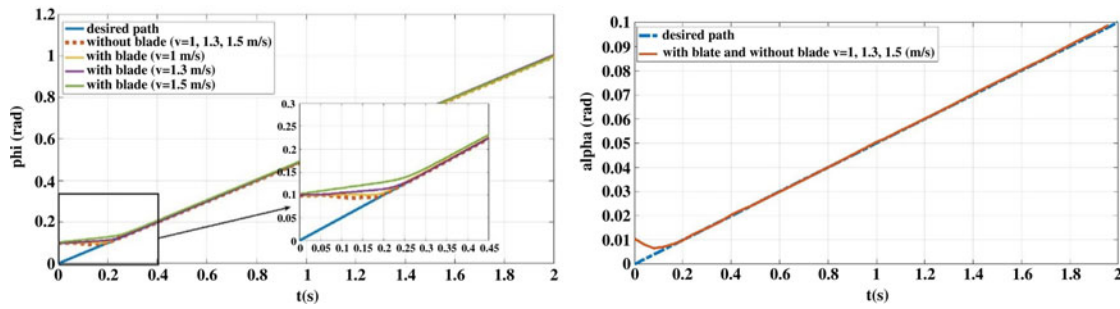


Fig. 7. The response of the robot joint space with different fluid velocities and its comparison between the simple robot and the one which is equipped by installed blades.

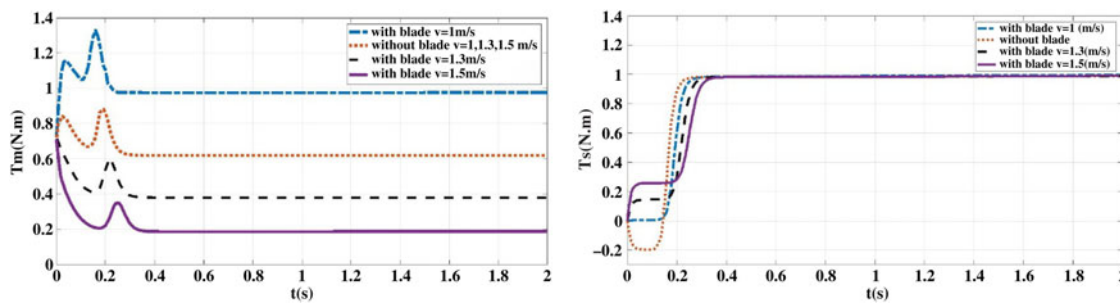


Fig. 8. Required controlling input of the robot joint space with different fluid velocities and its comparison between the simple robot and the one which is equipped by installed blades.

In the end, the required controlling input of the system is compared between the system with and without the turbine blade to extract the effect of installing the blades on energy consumption of the system.

The first Fig. 8 shows the comparison of the first input for these two systems. It can be seen that for higher speeds, the amount of required motor torque is less and considering the fact that the first state is almost similar for both cases, it can be concluded that a significant amount of energy is saved through the fluid stream. Also, it can be seen that the simple robot in which no blade is installed for, the maximum amount of energy is consumed. Thus, the amount of optimization range is about 20–50% for different speeds. Considering the fact that the difference in consuming force between different fluid speeds for the simple robot is not significantly huge, this item is not depicted here.

### 3.2. Optimal path planning using variation method

In this section, an optimal path is extracted between two arbitrary initial and final points and the states and their corresponding controlling inputs are compared to a simple arbitrary path between the same boundary conditions. In this scenario, the robot is supposed to move through the following initial and final states during the 1-s interval:

$$X = \begin{Bmatrix} \phi \\ \dot{\phi} \\ \alpha \\ \dot{\alpha} \end{Bmatrix}; X_0 = \begin{Bmatrix} 0 \\ 0 \\ 0.08 \\ 0 \end{Bmatrix} \rightarrow X_f = \begin{Bmatrix} 0.35 \\ 0 \\ 0.12 \\ 0 \end{Bmatrix} \quad (25)$$

It can be seen that the robot starts from rest and stops at the final position. Simultaneous solving of the state space together with the equations related to co-states, the optimal path between the initial and final points of Eqs. (19–21) can be extracted as Fig. 9 follow by the aid of BVP4C command of MATLAB.

It can be seen that as it was expected all of the states' movement are S shape which is according to the optimal variation in a state related to a system which has a dynamical differential equation of order two. In order to verify the optimality of the extracted path, the path is tracked, using the



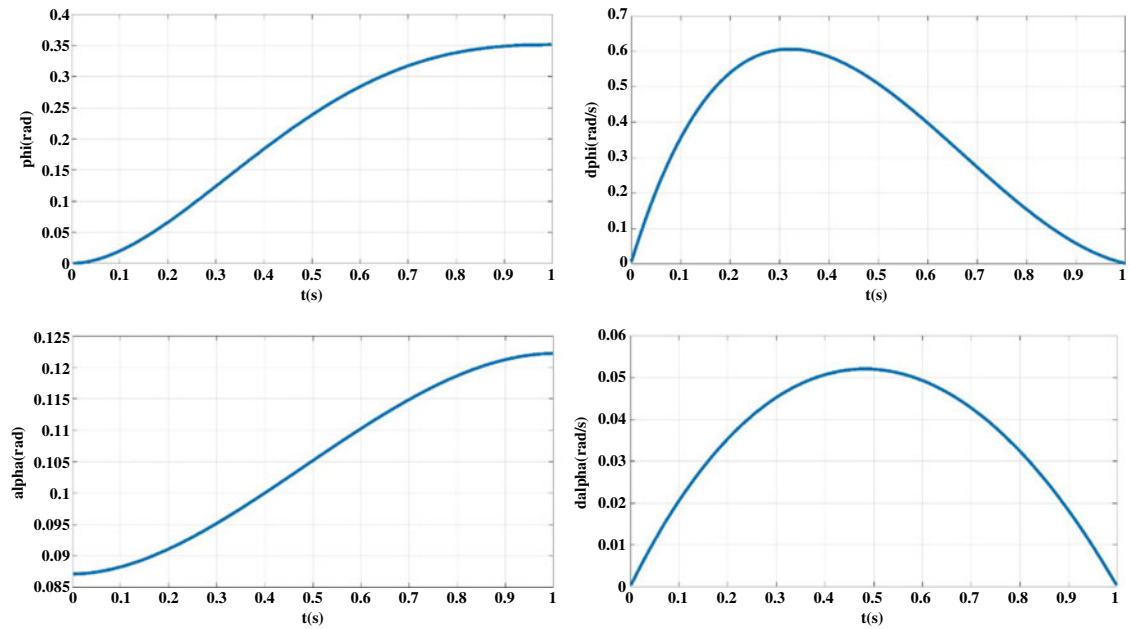


Fig. 9. The optimal path of the states.

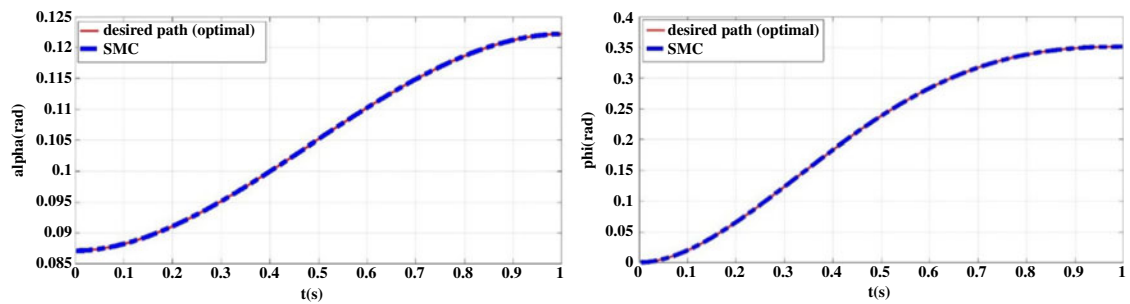


Fig. 10. Tracking the extracted optimal path by the aid of the sliding mode controller (SMC) controller for the first and third states.

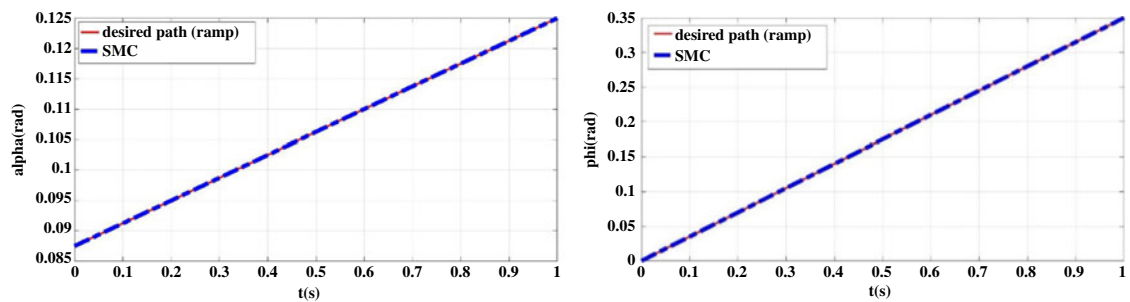


Fig. 11. Tracking the simple ramp path by the aid of the sliding mode controller (SMC) controller for the first and third states.

designed robust controller, and the related controlling inputs are compared with a manual path which is according to ramp inputs (Figs. 10 and 11).

Comparison of the controlling input between the extracted optimal path and the manual ramp one is depicted in Fig. 12.

It can be observed that the required controlling input is significantly decreased for the optimal path especially for the initial intervals of the movement while the same boundary conditions are satisfied. So it can be concluded that the designed optimal path generator together with the proposed robust

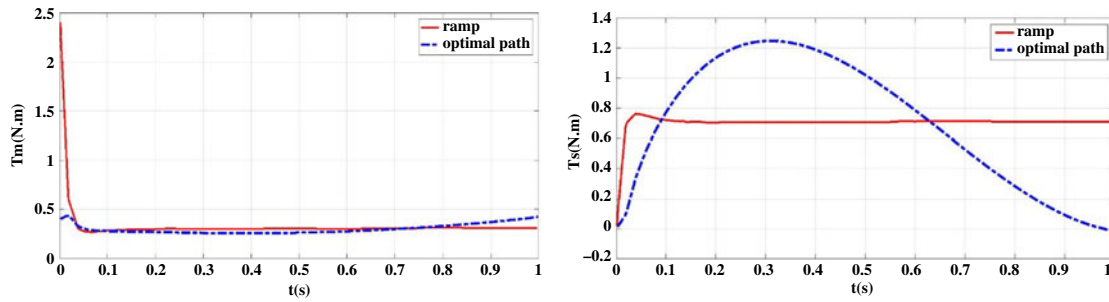


Fig. 12. Comparison of the controlling inputs ( $T_s, T_m$ ) between the optimal path and the ramp one.

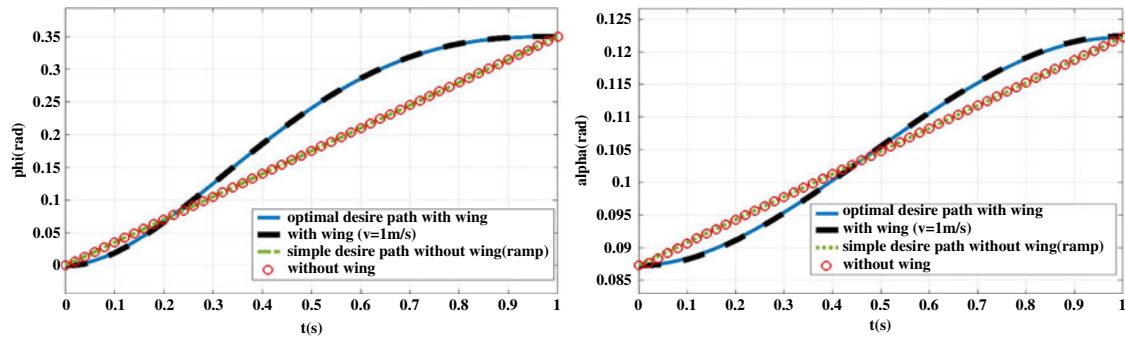


Fig. 13. Comparing the degrees of freedom (DOF) between the simple robot with optimal path and the robot equipped by blades in a straight path.

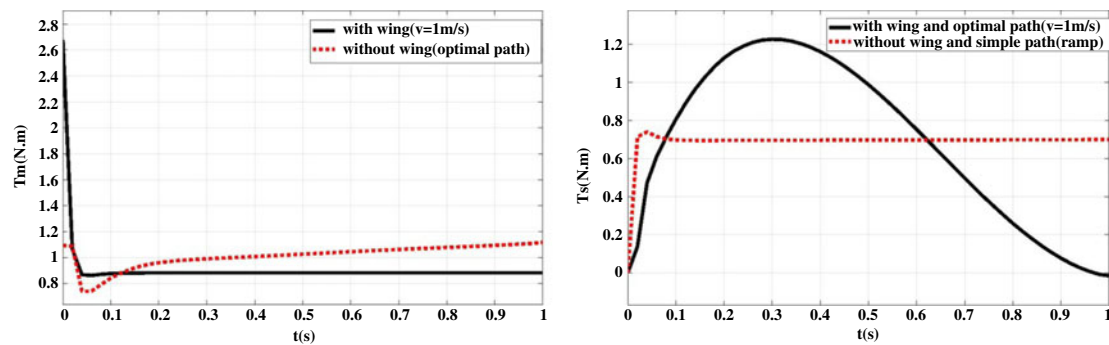


Fig. 14. Comparing the required motor torque between the simple robot with optimal path and the robot equipped by blades in a straight path.

controller can provide an optimal robust controller through which any arbitrary movement between the boundary conditions can be covered using the least amount of consumed energy.

### 3.3. Comparison and analysis

Now we analyze another scenario through which the optimality of the two presented methods is compared together. Here, first the optimal path is generated between two desired boundary points and its related kinetic inputs are extracted. Afterward, a straight path is tracked between the same boundaries but for a robot equipped by turbine blades and the results are compared together. Suppose that the initial and final boundaries are the same as Eq. (25). The states can be compared as seen in Fig. 13.

It can be seen that the optimal path generated using variation as was expected has a S-shaped curvature profile extracted by solving the HJB equation while the path used for the robot with blades is a simple linear movement between the boundaries. Comparing the required motor torque to track the path is as Fig. 14.

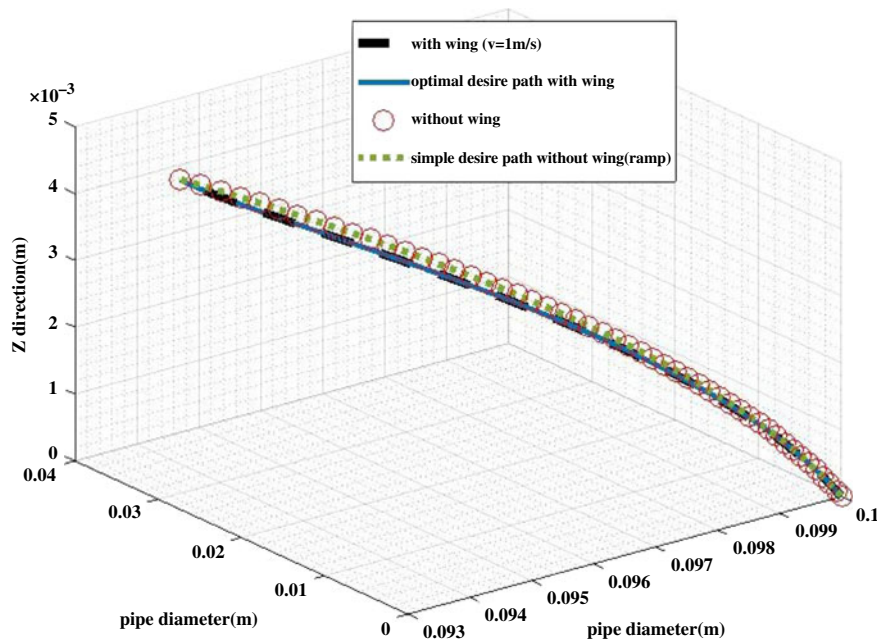


Fig. 15. Comparing the 3-D path of the four mentioned trajectories.

It is obvious that especially for the first input which is related to the propulsion of robot, though the optimal path causes the torque input to be minimized for the first time interval; however, after a specific time, it has been beaten as a result of the continuous drag force exerted by the stream. On the other hand, for the system for which the blades are installed with an optimum angle, putting aside the first intervals of the movement in which the time delay of optimality of the optimized dynamic of the system is not yet passed (about 0.1 s), the rest of the movement needs lower amount of controlling effort since the structure of the robot is improved in a way that results in a more optimum dynamics. This improvement, in this case, is about 30%.

Thus, it can be concluded that optimization of the dynamic structure of a system results in an improvement in the steady-state response of the system, while optimization in the solution of the dynamic equation results in decreasing the input in the transient response of the system. The second input which is related to the steering of the system is more dependent on the selected path but again the area under the profile is somehow similar for both cases. The 3-D comparison of the four different described paths can be observed in Fig. 15. Also notice that the energy harvesting can minimize the energy for any desired input, while in the HJB method the optimization needs to be regenerated for any new boundaries.

And in the final scenario, the response of the best case, that is, the robot equipped by turbine blades for which the optimal path is generated is compared with the worst case, that is, the simple robot for which its movement input is fed randomly as a linear input and the results are compared and analyzed. For the same boundary condition of Eqs. (19–21) as the previous scenario, the comparison of the trajectory for the optimal system with optimal path and the simple system with the random path can be depicted as below. It can be seen that here again the optimal path is a S-shaped trajectory which is realized by the aid of the designed controller and the random path is considered a linear function (Fig. 16).

Its related 3-D profile of trajectory can also be seen in Fig. 17.

Comparison of the required motor torque for both motors is extracted which can be seen in Fig. 18. Here it can be seen that as it was expected, for the first input which is related to the propulsion system, not only the required torque is less at the initial intervals of motion for the system equipped by the turbine blade in the optimal path, but also this optimality is continued for the rest of the movement. This is contributed to the fact that here both of the dynamic equation and also the dynamic solution are optimized simultaneously. As a result again here more than 50% decrease can be observed for the propulsion input.

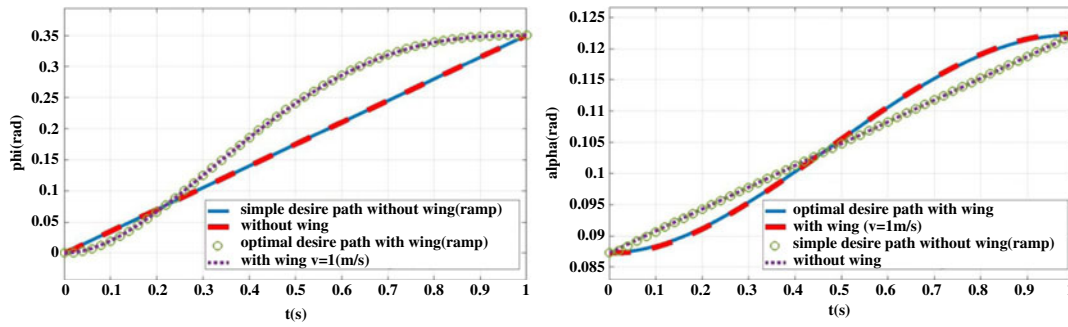


Fig. 16. Comparing of the trajectory between the simple robot with a random path and the robot equipped by blades in the optimal path.

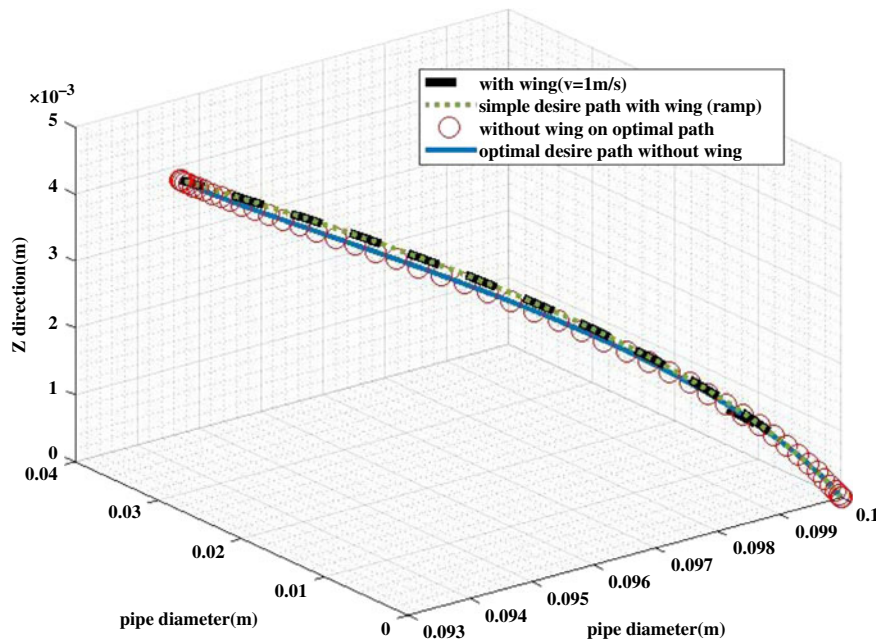


Fig. 17. Figure 3-D Comparison of the trajectory between the simple robot with a random path and the robot equipped by blades in the optimal path.

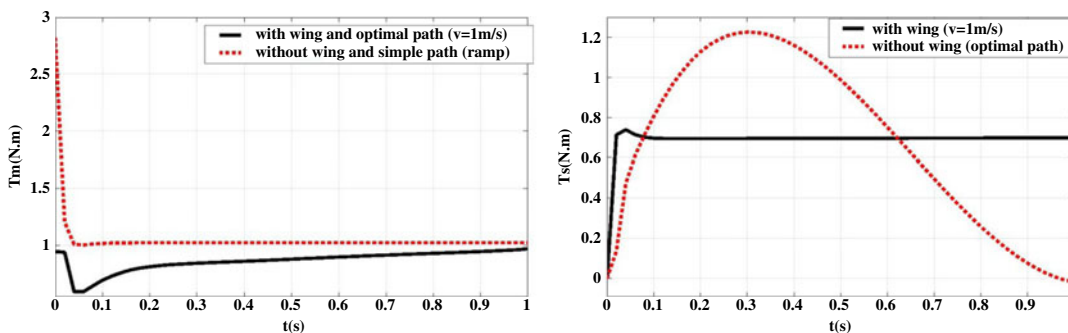


Fig. 18. Comparing the required motor torque between the simple robot with a random path and the robot equipped by blades in the optimal path.

Table II. The value of the physical parameters of the system for comparison.

Physical properties of the system			
Symbol	Value	Definition	Unit
$\lambda$	2.01	Total mass	Kg
$r$	0.02	Wheel radius	m
$b$	0.075	Pipe radius	m
$F_N$	35	The normal force of passive spring	N
$\mu$	0.3	Friction longitudinal coefficient	–
$i$	111	Gear ratio	–

About the second input, it can be seen that no extreme difference can be observed and this phenomenon can be justified, considering the fact that this input is related to steering and is extremely dependent on the selected path. Thus, since the optimal path is a curvature one, the related input has also harmonic shape; however, here again the area under the profile is roughly the same for both of the cases.

### 3.4. Verification and efficiency investigation

In this section, the correctness of modeling, robustness of the designed SMC controller, and efficiency of the proposed in-pipe robot equipped by turbine blades toward saving the energy is investigated by comparing the results with.<sup>35</sup> Engaged parameters for conducting the comparison study are as Table II.

At the first step, the kinematic and kinetic parameters of this reference are considered and the electrical required input energy is compared between the modeled robot of this paper and the one which is modeled in this reference. The desired trajectory is:

$$\dot{z} = 0.18 \sin\left(\frac{\pi}{10}t\right); \alpha = 15^\circ \quad (26)$$

Required mechanical energy is computed here by multiplication of the angular velocity of the motors provided from the kinematics of the robot according to Eq. (1) by the required motors' torque provided from kinetic of the robot according to Eq. (20). The resultant mechanical energy of the system then needs to be converted to the required electrical energy by dividing the computed mechanical energy by the efficiency of the robot provided in ref. [35].

$$\begin{aligned} E_m &= \dot{\phi} T_m \\ E_e &= E_m / \eta_m \end{aligned} \quad (27)$$

where  $E_m$ ,  $E_e$  are the mechanical and electrical energy of the robot and  $\eta_m$  is the efficiency of the motor. Comparison of the required electrical energy for the mentioned path and robot parameters is as follow (Fig. 19).

It can be seen that the profiles' trend are roughly similar which shows the correctness of modeling the system. The little difference between the profiles is contributed to the motor efficiency which is time dependent according to<sup>35</sup> while here we considered its average value.

At the second comparison, the required electrical energy is compared for the same trajectory and properties between a simple robot and the proposed robot equipped by turbine blades in the presence and absence of flowing fluid. This comparison is depicted in Fig. 20. As can be seen, the simple robot in the presence of fluid needs more energy which is obviously related to drag force of the flowing fluid. However, this fluid flow is employed in a profitable way in the proposed in-pipe robot equipped by turbine blades, while the consumed energy is significantly decreased by about 44%. This tremendous reduction in energy consumption shows the inevitable efficiency of the proposed in-pipe robot toward energy optimization.

In order to check the robustness of the designed controller against the external disturbances and parametric uncertainties related to the flowing fluid, the following desired path is considered:

$$\begin{aligned} \phi &= 3 \sin\left(\frac{\pi}{4}t\right); \phi_0 = 0.1 \text{ rad} \\ \alpha &= 0.015t + 5\pi/180; \alpha_0 = 7\pi/180 \end{aligned} \quad (28)$$



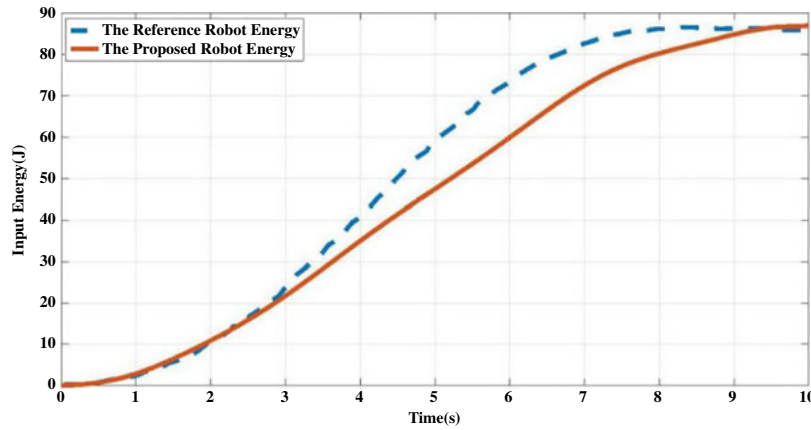


Fig. 19. Comparing the electrical consumed energy between the present paper and ref. [35].

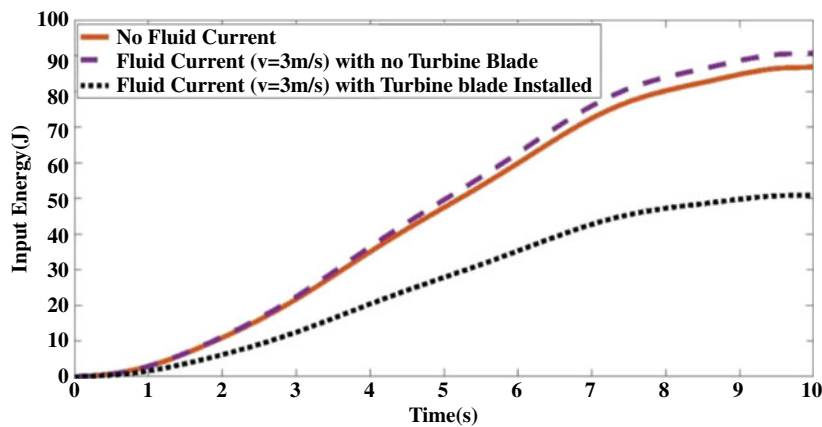


Fig. 20. Comparing the electrical consumed energy between the simple robot and the proposed one equipped by turbine blades in the presence and absence of fluid.

Following disturbance on the state  $\phi$  is supposed to be compensated by the aid of the designed SMC:

$$dis = 0.1 \sin(5t) \tag{29}$$

Also, it is supposed that the velocity of the fluid and the normal force of the robot suspension are not estimated correctly and the following parametric uncertainties are engaged:

$$\begin{cases} |v - \hat{v}| \leq 1 ; \hat{v} = 1 \text{ m/s} \\ |F_N - \hat{F}_N| \leq 15 ; \hat{F}_N = 20 \text{ N} \end{cases} \tag{30}$$

where  $\hat{v}, \hat{F}_N$  are nominal values of fluid velocity and normal force of wheels, respectively. Comparison of the actual path with respect to the desired one between the designed SMC method and simple feedback linearization (FBL) controller is depicted in Fig. 21. It can be seen that the regulation process of SMC is overdamped and it tracks the desired path precisely with a short settling time, while the actual path of the system controlled by FBL in underdamped has bigger settling time for both of the DOF as a result of the implemented disturbance and uncertainty.

The corresponding error comparison is shown as follow (Fig. 22).

As can be seen, the implemented uncertainties and disturbance on the first state affects the error of the third one since the corresponding states are coupled. Besides, it can be seen that as mentioned, the overshoot amplitude of the system controlled by SMC is significantly lower than FBL and its related settling time is decreased more than 90%. Also, the oscillatory response of the FBL, which is contributed to the implemented harmonic disturbance and is efficiently compensated by the aid of the

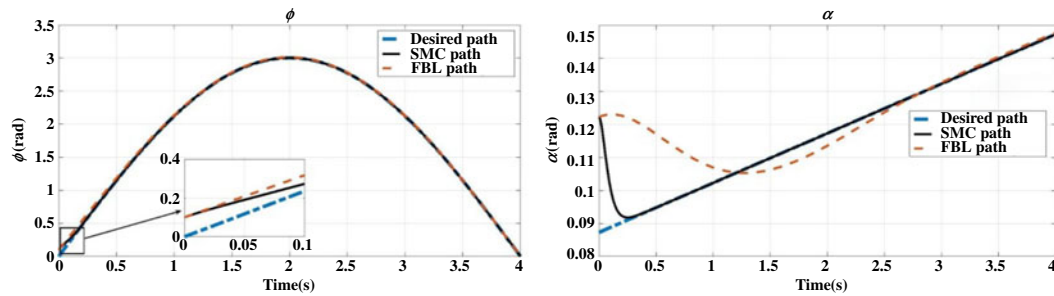


Fig. 21. Comparing the states between sliding mode controller (SMC) and FBL.

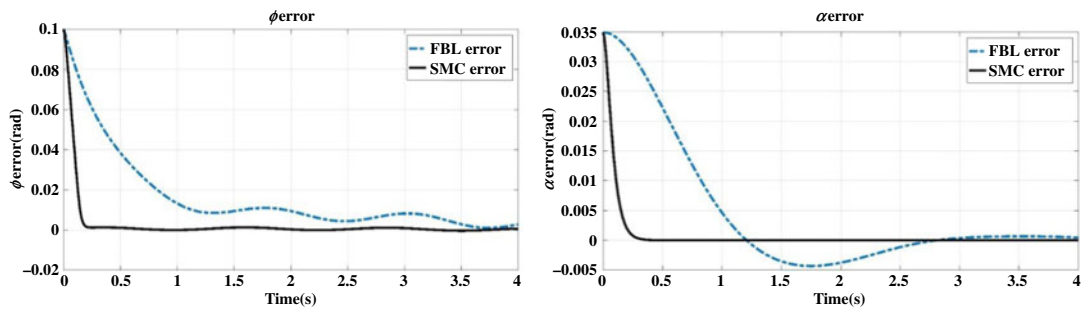


Fig. 22. Comparing the errors between sliding mode controller (SMC) and feedback linearization (FBL).

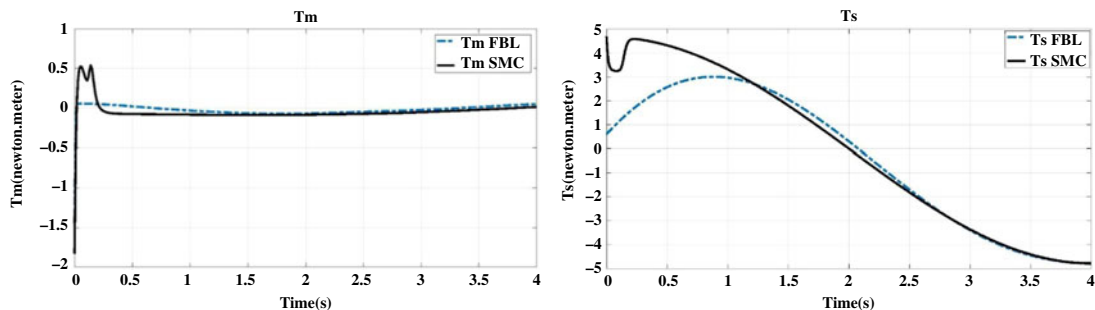


Fig. 23. Comparing the controlling inputs between sliding mode controller (SMC) and feedback linearization (FBL).

designed robust controller of SMC. The corresponding comparison of the controlling input between the mentioned controllers are depicted in Fig. 23.

It can be seen that the SMC has exerted oscillatory torque with respect to the required motor torque of FBL during the regulation process and this fact contributed to the implemented disturbance which is harmonic and this vibrating unwanted torque needs to be compensated by oscillatory exerted torque of the robust SMC. Also since the model has uncertainties, the mean value of the required motors' torque of SMC differs from the related value of FBL, especially for the third state.

#### 4. Conclusion and Discussion

In this paper, two different strategies of controlling effort optimization were investigated and implemented for a novel mechanism of screw locomotion in-pipe inspection robot with steerable capability. Kinematics, kinetics, and robust control of this robot were re-driven for a steerable version of the robot through which the pitch rate is varied by active control of the front wheel. The correctness of modeling was verified by comparing the results of MATLAB and ADAMS and its good compatibility confirmed the mentioned correctness. Afterward, a new method of energy harvesting was proposed for the cases in which the robot is supposed to move through the live pipes with flowing fluid pressure by installing turbine-shaped blades on the robot and using the drag force of the fluid pressure. The

formulation was updated for this special case and it was shown that not only for the cases in which the direction of the robot movement does agree with the direction of the fluid stream but also for the cases in which the direction is opposite, a significant improvement in input signal can be observed. The efficiency of the proposed optimization algorithms was checked by conducting some analytic and comparative simulation scenarios. It was explained that this improvement is the result of optimum dynamic design and installation of the blades on the main body of the robot, however, the value of this optimization percentage is dependent to the fluid velocity. It was shown that the more the fluid velocity, the more optimization percentage can be achieved which was about 20–50% in different speeds for the worst case in which the direction of the robot and the stream movement are opposite to each other. For the second approach, the optimization was performed as an optimal path planning for the robot between two specific boundaries using variation method without changing the physical design of the robot. It was again proved that for the mentioned case study, the same regulation accuracy can be covered by the aid of the proposed optimization approach while the consumed input can be decreased at the initial moments of the movement. This phenomenon is related to the fact that the optimization is performed just for solving the same differential equation, while the dynamic system itself is the same as before. At the next scenario in order to compare the efficiency of the two proposed optimization methods, the response of the simple robot in the optimal path was compared to the response of the system equipped by the turbine blades while tracks a random path. It was seen that as a result of optimizing the solution of the differential equation for the optimal path, the required input is less for the initial moments while for the rest of the movement, the optimization on the differential equation, that is, installing the blades on the robot overcome the former optimization method by about 30%. So it can be concluded that the former optimization method, that is, installing blades on the robot result in a steady-state optimization of input while for the latter case that is, calculating the optimal path, transient optimization can be observed. Furthermore optimization of the robot hardware results in the energy reduction of any path while for the HJB method, the optimum path should be regenerated for any new boundaries. At the final scenario, the response of the best case, that is, the robot with blades in the optimal path is compared with the response of the worst case and as it was expected here for the propulsion input both of transient and steady-state responses are optimized simultaneously for the optimized case by about 50%. These results are related for the first input which is related to the propulsion of the system and the variations in the second input profile, which is related to steering, is extremely dependent on the selected path and are roughly similar for both cases. All of the mentioned theories were verified using MATLAB simulation and comparative analysis. Also, the correctness of modeling and superiority of the proposed in-pipe robot with respect to other traditional cases were verified by comparing the results with previous research, and it was shown that the energy consumption for a special case study can be reduced by up to 44%. It was also proved that the designed SMC controller is robust against the external disturbances and can decrease the errors' settling time more than 90% with respect to FBL which is not robust. Thus, using the proposed design and controlling strategies of this paper for the in-pipe robot, a steerable movement of this robot is possible through the pipeline with obstacle avoidance capability, while the least amount of energy consumption is required for a specific path for the former method and between two specific boundaries for the second approach.

### Conflict of Interest

The authors declare that they have no conflict of interest.

### References

1. Z. Peng, S. Yang, G. Wen, A. Rahmani and Y. Yu, "Adaptive distributed formation control for multiple non-holonomic," *Neurocomputing*, **173**, 1485–1494 (2015).
2. G. Scaglia, E. Serrano, A. Rosales and P. Albertos, "Linear interpolation based controller design for trajectory tracking under uncertainties: application to mobile robots," *Control Eng. Pract.* **45**, 123–132, (2015).
3. K. R. Simba, N. Uchiyama and S. Sano, "Real-time smooth trajectory generation for nonholonomic mobile robots using Bézier curves," *Robot. Comput.-Integ. Manuf.* **41**, 31–42 (2016).
4. V. F. Filaretov and V. E. Pryanichnikov, "Autonomous mobile university robots AMUR: Technology and applications to extreme robotics," *Procedia Eng.* **100**, 269–277, (2015).
5. T. Liu and Z. P. Jiang, "Distributed formation control of nonholonomic mobile robots without global position measurements," *Automatica*, **49**(2), 592–600 (2013).

6. M. Takahashi, I. Hayashi, N. Iwatsuki, K. Suzumori and N. Ohki, "The development of an in-pipe micro robot applying the motion of an earthworm," *Seimitsu Kogaku Kaishi*, **61**, 90–94 (1995).
7. K. Suzumori, S. Wakimoto and M. Takata, "A Miniature Inspection Robot Negotiating Pipes of Widely Varying Diameter," *2003 IEEE International Conference on Robotics and Automation (Cat. No. 03CH37422)*, Taipei, Taiwan (IEEE, 2013) vol. 2, pp. 2735–2740.
8. A. Zagler and F. Pfeiffer, "(MORITZ) a pipe crawler for tube junctions," *Robot. Automat.*, **3**, 2954–2959 (2003).
9. J. H. Kim, G. Sharma and S. S. Iyengar, "FAMPER: A Fully Autonomous Mobile Robot for Pipeline Exploration," *2010 IEEE International Conference on Industrial Technology*, Vina del Mar (IEEE, 2010) pp. 517–523. IEEE.
10. P. Harish and V. Venkateswarlu, "Design and motion planning of indoor pipeline inspection robot," *Int. J. Innovat. Technol. Explor. Eng. (IJITEE)*, **3**(17), 7 (2013).
11. K. Suzumori, T. Miyagawa, M. Kimura and Y. Hasegawa, "Micro inspection robot for 1-in pipes," *Mechatronics*, **4**(3), 286–292 (1999).
12. K. Nagaya, T. Yoshino, M. Katayama and I. Murakami, "Wireless piping inspection vehicle using magnetic," *IEEE/ASME Trans. Mechatron.* **17**(3), 472–479 (2012).
13. M. Ciszewski, T. Buratowski, M. Giergiel and P. Małka, "Virtual prototyping design and analysis of AN in-pipe inspection mobile robot," *Theor. Appl. Mech.* **52**(2), 417–429 (2014).
14. Y. Kwon and B. Yi, "Design and motion planning of a two-module collaborative indoor pipeline inspection robot," *IEEE Trans. Robot.* **28**(3), 681–696 (2012).
15. J. Park, D. Hyun, W. H. Cho, T. H. Kim and H. S. Yang, "Normal-force control for an in-pipe robot according to the inclination of pipelines," *IEEE Trans. Indust. Electron.* **58**(12), 5304–5310 (2011).
16. Y. Zhang and G. Yan, "In-pipe inspection robot with active pipe-diameter adaptability and automatic tractive force adjusting," *Mech. Mach. Theory* **42**(12), 1618–1631 (2007).
17. S. Roh and H. R. Choi, "Differential-drive in-pipe robot for moving inside urban gas pipelines," *IEEE Trans. Robot.* **21**(1), 1–17 (2005).
18. E. Dertien, M. M. Fomashi, K. Pulles and S. Stramigioli, "Design of a Robot for In-pipe Inspection Using Omnidirectional Wheels and Active Stabilization," *2014 IEEE International Conference on Robotics and Automation (ICRA)*, Hong Kong, China (IEEE, 2014) pp. 5121–5126.
19. P. Li, S. Ma, B. Li and Y. Wang, "Multifunctional Mobile Units with a Same Platform for In-pipe Inspection Robots," *In 2008 IEEE/RSJ International Conference on Intelligent Robots and Systems*, Nice, France (IEEE, 2008) pp. 2643–2648.
20. A. Kakogawa and S. Ma, "Mobility of an in-pipe robot with screw drive mechanism inside curved pipes," *Robotics and Biomimetics (ROBIO)* (2010) pp. 1530–1535.
21. Y. Zhang, M. Zhang, H. Sun and Q. Jia, "Design and Motion Analysis of a Flexible Squirm Pipe Robot," *2010 International Conference on Intelligent System Design and Engineering Application*, Changsha (IEEE, 2010) vol. 1, pp. 527–531.
22. T. Li, S. Ma, B. Li, M. Wang and Y. Wang, "Control strategies of energy optimization for an in-pipe robot with inclining-angle-adjustable screw rollers," *J. Mech. Eng.* **50**(17), 8–16 (2014).
23. M. H. Korayem, M. Irani and S. Rafee Nekoo, "Motion control and dynamic load carrying capacity of mobile robot via nonlinear optimal feedback," *Manuf. Mater. Sci.* **2**(1), 1 (2012).
24. A. Abbaspour, K. Alipour, H.Z. Jafari, S. Ali and A. Moosavian, "Optimal formation and control of cooperative wheeled mobile robots," *Comptes Rendus Mécanique* **343**(5–6), 307–321 (2015).
25. M. Boukens, A. Boukabou and M. Chadlib, "Robust adaptive neural network-based trajectory tracking control approach for nonholonomic electrically driven mobile robots," *Robot. Auton. Syst.* **92**, 30–40 (2017).
26. J. Krishnan, U. P. Rajeev, J. Jayabalan and D. S. Sheela, "Optimal motion planning based on path length minimisation," *Robot. Auton. Syst.* **94**, 245–263 (2017).
27. J. Han and Y. Seo, "Mobile robot path planning with surrounding point set and path improvement," *Appl. Soft Comput.* **57**, 35–47 (2017).
28. R. Z. Song, W. D. Xiao and C. Y. Sun, "Optimal tracking control for a class of unknown discrete-time systems with actuator saturation via data-based ADP algorithm," *Acta Automatica Sinica* **39**(9) 1413–1420 (2013).
29. D. M. Adhyaru, I. N. Kar and M. Gopal, "Bounded robust control of nonlinear systems using neural network-based HJB solution," *Neural Comput. Appl.* **20**(1), 91–103 (2011).
30. A. Sioma, "Biologically-inspired water propulsion system," *J. Bionic Eng.* **10**(3), 274–281 (2013).
31. B. Allotta, R. Costanzi, N. Monni, L. Pugi, A. Ridolf and G. Vettori, "Design and simulation of an autonomous underwater vehicle," *ECCOMAS*, Vienna, Austria (2012).
32. E. Zakeri, S. Farahat, S.A. Moezi and A. Zare, "Robust sliding mode control of a mini unmanned underwater vehicle equipped with a new arrangement of water jet propulsions: Simulation and experimental study," *Appl. Ocean Res.* **59**, 521–542 (2016).
33. E. A. Baskharone, *Principles of Turbomachinery in Air-Breathing Engines* (Cambridge University Press, 2006).
34. H. Tourajizadeh, M. Rezaei and A. H. Sedigh, "Optimal control of screw in-pipe inspection robot with controllable pitch rate," *J. Intell. Robot. Syst.* **90**(3–4), 269–286 (2018).
35. P. Li, S. Ma, C. Lyu, X. Jiang and Y. Liu, "Energy-efficient control of a screw-drive pipe robot with consideration of actuator's characteristics," *Robotics Biomim.* **3**(1), 11 (2016).